

May 2020

Monitoring CO2 underground storage with the
Riccati equation

Paper no. 2

Cand. Real. Knut Sørsdal

Norway, 2020

Abstract

A study is made of an inversion technique of the Riccati type applied to a CO₂-plume on the Sleipner field in the North sea. This paper employs Q-models to introduce forward and inverse filtering of the data. The solution of the Riccati equation with the the Kolsky-Wang Q-model has been presented in previous papers and is applied here. The linear solution of the wave equation introducing attenuation and dispersion has been studied by Wang. He used a modification of Kolsky's Q-model and applied it on a downward continuation algorithm. I have taken the theory further with a general Q-model and a more elegant inversion. The theory is applied on real seismic data from the Sleipner field.

The background model

Higher amounts of CO₂ in the atmosphere has contributed to finding techniques to mitigate the emissions of CO₂. One of those techniques is Carbon Capture and Storage (CCS). CO₂ can be stored in subsurface reservoirs over time. Monitoring and modeling of reservoirs is important to avoid leakage and to predict how the CO₂ could migrate. Modeling is also useful when the seismic interpreter needs a close look at the subsurface data. Then seismic from modeling with known parameters can be useful. I have used the Riccati-equation both for modeling and for inversion to recover the original data used in the seismic theory.

I will connect my theory to real data, and the first place in the world to inject CO₂ was at the Sleipner field in the Norwegian North Sea. The injection found place in 1996 in the Sleipner East field into the Utsira formation. The reservoir is estimated to have a vertical thickness about 200 m at the injection point, and the estimated caprock for the CO₂ is about 100 m thick.

So, this article shows modeling of the seismic response from different synthetic models associated with CO₂ underground storage where the parameters are based on real data.

CO₂ saturation, geometry of the models and some other things are all important parameters affecting the seismic result. I have done calculations with a background model that is saturated with CO₂ and received different results depending on some simple parameters.

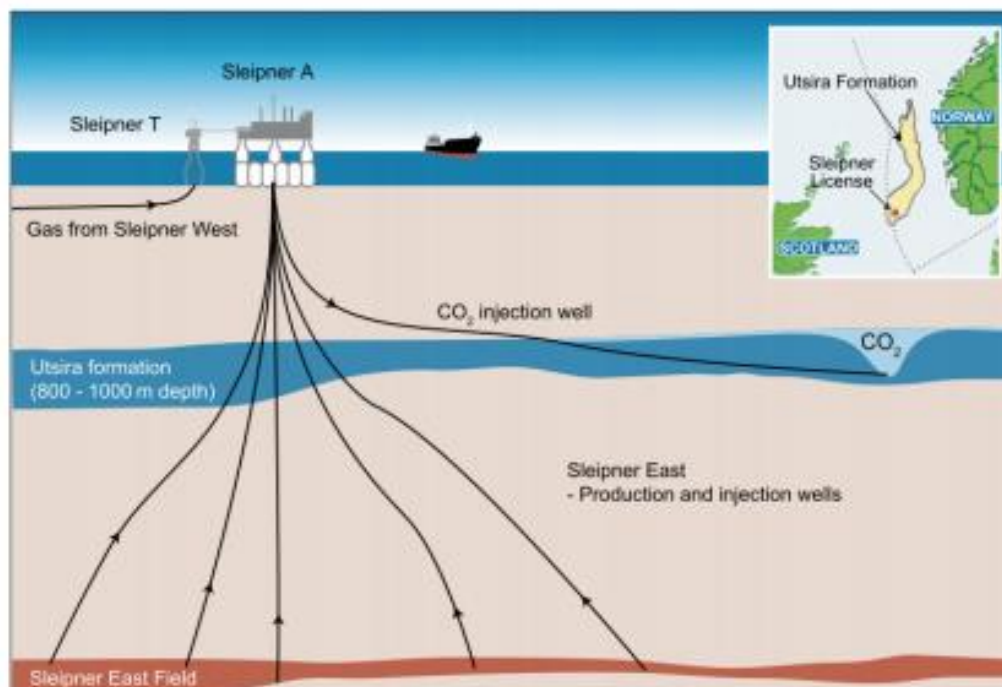


Figure 1. Utsira formation (from IPCC 2005)

Introduction to seismic

Seismic inverse Q-filtering (IQF) is one sector of regular inversion technics that employs a wave propagation reversal procedure that compensates for energy absorption and corrects wavelet distortion due to velocity dispersion. When modelling for the inversion we introduce forward Q-filtering (FQF) models, and will give a short description of the background for such models.

Actually, there is a wide range of mathematical definitions of the Q-model presented in the literature, and Wang (2008) summed up about this. A good start is the Kolsky (1953) model that is used extensively in Q-filtering. Wang proposed to modify the Kolsky's basic attenuation-dispersion model. This was primary an attempt to accurately represent the velocity dispersion effect within the seismic frequency band.

Wang writes that if one compares the basic Kolsky model with other different mathematical Q models, one finds that different models were not close to the basic Kolsky model. Wang, by using a modified Kolsky model, was able to derive a set of analytically derived parameters. The primary goal was to make Kolsky's model comparative with a model satisfying a dispersion condition that is necessary to preserve the causality of a propagating wavelet. Such a dispersion relation is called the Kramers-Krönig dispersion relation. A model of this kind has been discussed by Futterman (1962).

I will use both these Q-models in this article. However, to avoid a rather complicated inverse theory, I will use a least square (LSQ) solution in the Riccati inversion to replace Wang's inverse Q-filtering theory with downward continuation. An attempt with this inversion method without the LSQ-solution was done by Gjevik et al. (1975). In another article Nilsen and Gjevik (1978) presented the theory in a broader way and one absorption model was included. Their theory has been further developed and was presented in the two papers on Researchgate mentioned above.

We will briefly recapitulate their theory by introducing a general absorption model in a forward modelling approach. From this general model we will end up with Q-models of which one will be used in modelling for the inversion as was done in a previous paper, Sørdsdal (2019).

Basics of modelling with absorption included

Inverse Q-filtering algorithms are mainly based on forward wave propagation migration type approach. Then the decay of the frequency content due to absorption can be inspected at each time sample. (Wang (2008).) Following Gjevik we can assume monochromatic plane-waves propagating along a vertical axis. Let P define the stress (pressure) and W the displacement. Density is ρ . Newton's second law gives:

$$\frac{dP}{dz} + \rho \omega^2 W = 0 \quad (1)$$

Correspondingly, a stress-strain relationship of the following form is assumed (Hook's law):

$$P = \rho v_r^2 Y \frac{dW}{dz} \quad (2)$$

In Eq.(2) v_r is the reference velocity which could be taken as the group velocity in case of dispersion. The function Y represents depth and frequency-dependent absorption.

In case of no damping, $Y=1$ and Eq.(2) is simply Hookes law.

Combination of Eqs.(1) and (2.b) gives Helmholtz equation (assume constant density)

$$\frac{d^2 P}{dz^2} + k^2 P = 0, k = \frac{\omega}{v_r \sqrt{Y}} \quad (3)$$

To achieve a complex damping function we can follow Horton (1959) and introduce the notation

$$Y(\omega, \tau) = A(\omega, \tau) + iB(\omega, \tau) \quad (4)$$

In his paper, Horton gives examples of values of A and B for various absorption models that can be causal or non-causal. Since the wavenumber k is in focus, the following expression is now elaborated on

$$\frac{1}{\sqrt{Y}} = \frac{1}{\sqrt{A+iB}} = \frac{\sqrt{A-iB}}{\sqrt{A^2+B^2}} = \frac{(A^2+B^2)^{1/4} [\cos(u/2) - i \sin(u/2)]}{(A^2+B^2)^{1/2}} = \frac{[\cos(u/2) - i \sin(u/2)]}{(A^2+B^2)^{1/4}}$$

$$\tan(u) = \frac{B}{A} \quad (5)$$

Moreover, the following trigonometric relations are valid

$$\tan(u) = \frac{\sin(u)}{\cos(u)} = \frac{\sin(u)}{\sqrt{1-\sin^2(u)}} = \frac{\sqrt{1-\cos^2(u)}}{\cos(u)} = \frac{B}{A} \Rightarrow \quad (6)$$

$$\cos(u) = \frac{A}{\sqrt{A^2+B^2}}, \quad \sin(u) = \frac{B}{\sqrt{A^2+B^2}}$$

And also these

$$\cos(u/2) = \sqrt{\frac{1+\cos(u)}{2}}, \quad \sin(u/2) = \sqrt{\frac{1-\cos(u)}{2}} \quad (7)$$

Finally, combination of Eqs. (5)-(7) gives the result

$$k = \frac{\omega}{v_r \sqrt{Y}} = \frac{\omega}{v_r \sqrt{A+iB}} = \frac{\omega}{v_r} \left[\frac{1}{\sqrt{A}} - \frac{i}{2} \frac{B}{A\sqrt{A}} \right] \quad (8)$$

Now we will compare the real and imaginary part of k for the Q-models. The real part can be related to the phase velocity and the imaginary part is the attenuation coefficient. Then we have: $k_{real} = \frac{\omega}{v_r} \frac{1}{\sqrt{A}}$

and
$$k_{imag} = \frac{1}{2} \frac{\omega}{v_r} \frac{B}{A\sqrt{A}} \tag{9}$$

This leads up to different functions A and B that was calculated in Sørdsdal (2019) and can be related to Q-models. The outline is also given in appendix 1 and is listed in table 1.

		Kolsky Wang (FQF)	
		A	B
1	Kolsky - Wang	$\left[\frac{\omega}{\omega_h}\right]^{2\gamma} \gamma = \frac{1}{\pi Q}$	$\left[\frac{\omega}{\omega_h}\right]^{2\gamma} \frac{1}{Q}$

Table 1.

Fig.3. shows \sqrt{A} (which gives us a hint about the dispersion) for Kolsky-Wang. (Multiplying \sqrt{A} with the reference velocity v_r gives us the phase velocity). According to Kolsky, the tuning frequency ω_h should be the smallest frequency in the frequency band and. Wang modified the Kolsky model by choosing the highest frequency in the frequency band. And that will be the Nyquist frequency $2\pi\omega_h = 125$ Hz (blue graph on fig.3.)

For the attenuation coefficient Fig.2. we used $Q=100$ (blue graph) and $Q=50$ (green graph). The attenuation coefficient increase linear with frequency. An important aspect with the Kolsky model is that the attenuation will be strictly linear with frequency over the range of measurement.

From fig.3. we can readily see that more damping (red graph) gives the lower graph. This means that the less damping, the faster will go the reflectors. We will see this when we compute the synthetics.

Attenuation coefficient

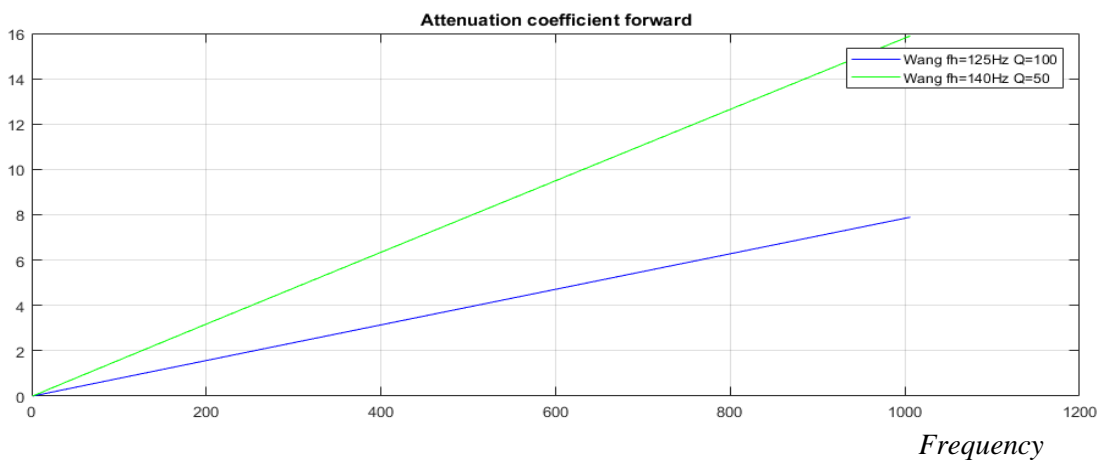


Fig.2. Attenuation coefficient. Attenuation coefficient is dimensioned pr. km or pr.sec.

Phase velocity

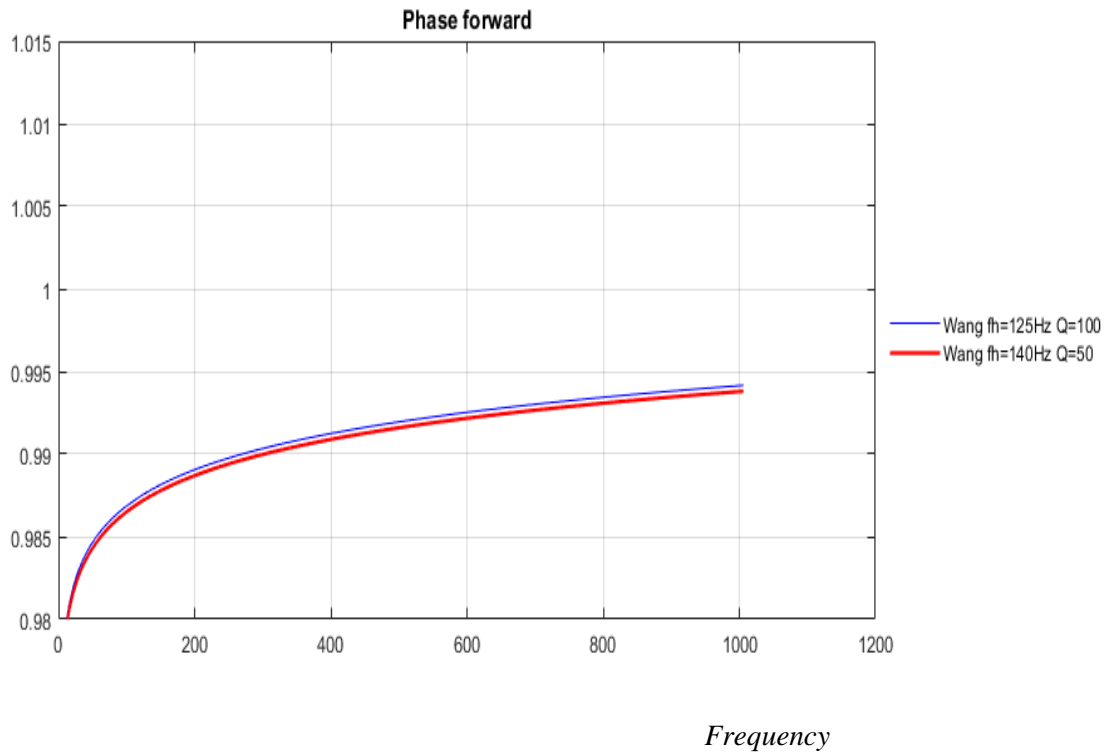


Fig.3. Phase velocity for forward Q -model of table 1. We have used $Q=50$. Wang $fh=140\text{Hz}$ (red) Wang $fh=125\text{Hz}$ (red) ($\omega_h=2\pi f_h$), $Q=100$. Phase velocity is dimensionless.

Introducing the Riccati equation with absorption

The basic idea in a downward wave propagation migration approach is that the wavefield at the surface of the seismic earth model is extrapolated down to a depth z . The real part of k in Eq. (9) describes all dispersion effects during wave propagation and the imaginary part describes absorption.

From Nilsen and Gjevik (1978) we have the Riccati equation:

$$\frac{dK}{dz} = \frac{2i\omega}{v_r \sqrt{Y}} K - r(1 - K^2) \quad (10)$$

K is the complex reflection coefficient and r is the depth-dependent ‘reflectivity’ per depth unity:

$$r(\tau) = \frac{1}{2\rho v_r} \frac{d(\rho v_r)}{d\tau} \quad (11)$$

Since vertically travelling waves are considered, the transformation from depth to two-way traveltme is straightforward

$$\tau = 2 \int_0^z \frac{dz}{v_r}, \Rightarrow d\tau = \frac{2}{v_r} dz \quad (12)$$

Which gives the travel time version of Eq.(10)

$$\frac{dK(\omega, \tau)}{d\tau} = \frac{i\omega}{\sqrt{Y(\omega, \tau)}} K(\omega, \tau) - r(\tau)(1 - K^2), r(\tau) = \frac{1}{2\rho v_r} \frac{d(\rho v_r)}{d\tau} \quad (13)$$

By noticing that

$\exp(-i\omega \int_0^\tau Y(\omega, \tau)^{-1/2} d\tau) \equiv \exp[-\phi(\omega, \tau)]$ is an integrating factor for this Riccati equation, it can be rewritten on the following form:

$$\frac{d}{d\tau} [K(\omega, \tau) \exp(-\phi(\omega, \tau))] = -r(\tau)(1 - K^2) \exp(-\phi(\omega, \tau)) \quad (14)$$

$$\text{Where } \phi(\omega, \tau) = i\omega \int_0^\tau \frac{d\tau}{\sqrt{Y(\omega, \tau)}} = i\omega \int_0^\tau \left[\frac{1}{\sqrt{A}} - \frac{iB}{2A\sqrt{A}} \right] d\tau = \int_0^\tau \left[\frac{i\omega}{\sqrt{A}} + \frac{\omega B}{2A\sqrt{A}} \right] d\tau \quad (15)$$

Assume now the following boundary condition: $K=0$ when $\tau \geq T$. Integration of Eq. (14) now gives the solution

$$-K(\omega, \tau) \exp(-\phi(\omega, \tau)) = -\int_\tau^T r(\tau') \exp(-\phi(\omega, \tau')) (1 - K^2(\omega, \tau')) d\tau' \quad (16)$$

From Eq.(16) we can, when $K^2 \ll 0$, obtain the non-linear solution

$$K(\omega, \tau) = \exp(\phi(\omega, \tau)) \int_\tau^T r(\tau') \exp(-\phi(\omega, \tau')) (1 - K^2(\omega, \tau')) d\tau' \quad (17)$$

Equation (17) is now the starting point for a non-linear modelling algorithm. Assume a discretization in τ (sample interval $\Delta\tau$ and total of N points), and then start at maximum time $T=(N-1) \Delta\tau$ and then calculate K in upward direction.

We introduce the following notation for convenience

$$K_{i,j}^n = K^n(\omega_i, \tau_j) \quad \tau_j = (j-1)\Delta\tau, j = N-1, N-2, \dots, 1 \quad (18)$$

$$K_{i,N}^n = 0$$

Where the superscript n implies iteration number.

Next, define (trapezoidal rule applied to integral in Eq.(17)) (assume $(n+1)$ th. iteration)

$$\beta_{i,j} = \frac{\Delta\tau}{2} \left[r_{j+1} X_{i,j+1} \{1 - (K_{i,j+1}^n)^2\} + r_j X_{i,j} \{1 - (K_{i,j}^n)^2\} \right], j = N-1, N-2, \dots, 1 \quad (19)$$

$$r_N = 0$$

Which gives the after sought solution

$$K_{i,j}^{n+1} = \beta_{i,j} / X_{i,j}, j = N-1, N-2, \dots, 1 \quad (20)$$

In Eqs.(18 and 19) we have introduced the operator

$$X_{i,j} = \exp[-\phi(\omega_i, \tau_j)] \tau_j = (j-1)\Delta\tau \quad (21)$$

The seismogram corresponds to the solution $j=1$. The final result in time is obtained after an inverse FFT.

Let the first layer be water, then we need to include the free-surface multiples. Assume that τ_w represents two-way vertical travel time in the water layer. Total field P_i recorded at the surface (e.g. including multiples) can then be written as (r being the reflection coefficient of the seafloor)

$$P_i = K_{i,j=1} \left[1 - r \exp(-i\omega_i \tau_w) + r^2 \exp(-2i\omega_i \tau_w) + \dots = \frac{K_{i,j=1}}{1 + r \exp(-i\omega_i \tau_w)} \right] \quad (22)$$

Forward numerical implementation

When we make calculations with the models we need to define $r(\tau)$ from a set of layered model parameters connected to the impedance of a seismic media. We can, of course, get r_j from eq (22) as reflectivity per depth unit (1/s). Invoking Eq.(23) we can calculate two-way traveltimes by converting the layer thickness z into time and using:

$$r(\tau) = \frac{1}{2(\tau_{j+1} - \tau_j)} \left[\frac{\rho_{j+1} v_{j+1}}{\rho_j v_j} - 1 \right] \quad j=1, \dots, NT-1 \quad (23)$$

We can then get R_j (Reflection coefficients) either by setting ρ and v direct into Eq.(24) or setting r from Eq (23) into Eq.(24). Both r and R are similar physical parameters which represents the contrast in acoustic impedance across an interface. To proceed with computations we must discretize every layer in the model with j and move down to the layer $NT-1$. Velocity and density for each layer we find in table 2.a and b:

$$R_j = \frac{\rho_{j+1} v_{j+1} - \rho_j v_j}{\rho_{j+1} v_{j+1} + \rho_j v_j} = \frac{\exp[2\Delta\tau r_{j+1}] - 1}{\exp[2\Delta\tau r_{j+1}] + 1} \quad \text{for } j = 0, 1, 2, \dots, NT-1 \quad (24)$$

To set up table 3 for our model parameters we need some data from the Sleipner field. These data we achieved from Nordahl (2015). Data are in table 2. The CO2-saturation is important when we study the CO2-plume Studying fig.4, we were able to set up a model roughly with CO2-layers 25 m thick and from fig.5 we could locate maximum saturation and put data into table 3. Figure 6 gave us an idea of absorption as a function of CO2 saturation.

CO ₂ saturation	P-velocity (m/s)
20 %	1568
50 %	1470
100 %	1437

Density (kg/m ³)	Acoustic impedance (Vp·ρ)
2030	$Z_2 = 3,183 \cdot 10^6$
2006	$Z_2 = 2,949 \cdot 10^6$
1965	$Z_2 = 2,824 \cdot 10^6$

Table 2. CO2 saturation, velocity, density and impedance from Nordahl (2015).

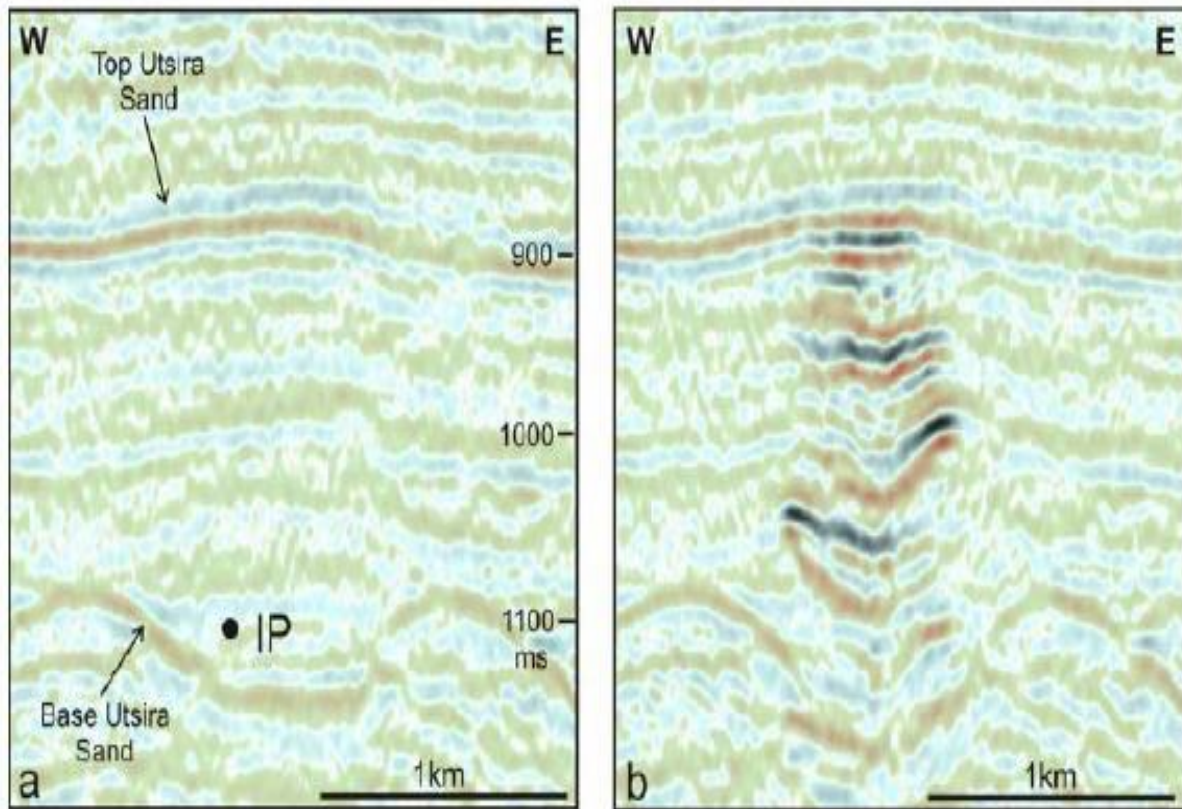


Fig.4.CO2 layers from Utsira sand, Sleipner field

Q	(Depth) Layers	Bgr.density ρ g/cm ³	Other densities	Bgr.velocity v km/h	Other. velocities	Saturation CO2	Depth	Layers
$Q1=100$	150	1.0	1.0	$V1=1480$	1480		80	Layer 1
$Q2=100$	250	1.965	1.5	$V2=1600$	1600		640	Layer 2
$Q3=100$	1000	1.965	2.0	$V3=2400$	600 800 1000		720	Layer 3 Caprock
$Q4=1000$	400	2.03	1.966	$V4=1470$	2000	100 %	820	Layer 4 CO2
$Q5=1000$	25	1.96	1.5	$V5=1500$	1500	25 %	875	Layer 5

Table 3.a. Seismic model parameters small model

D	= [150, 250, 1000, 400, 25]	%depth	[m]
V	= [1480, 1600, 2400, 1470, 1500]	%velocity	[m/s]
Rho	= [1, 1.965, 1.965, 2.03, 1.96]	%density	[g/cm ³]
Q1	= [1000, 1000, 1000, 1000, 1000]	% absorption	Q.
Q2	= [100, 100, 100, 1000, 1000]	% absorption	Q.

<i>Q</i>	<i>Depth)</i> <i>Layers</i>	<i>Density</i> ρ g/cm ³	<i>Bgr.</i> <i>dens.</i>	<i>Velocity v</i> km/h	<i>Backgr.</i> <i>velocity</i>	<i>Saturation</i> <i>CO2</i>	<i>Depth</i>	<i>Layers</i>
<i>Q1=200</i>	80	1.0	1.0	<i>V1=1480</i>	1480	0 %	80	Water layer
<i>Q2=200</i>	560	1.5	1.5	<i>V2=1600</i>	1600	25 %	640	Layer 2
<i>Q3=200</i>	80	2.0	2.0	<i>V3=2000</i>	2000	25 %	720	Layer 3
<i>Q4=200</i>	155	2.03	2.0	<i>V4=1800</i>	1800	25 %	875	Layer 4
<i>Q5=200</i> <i>100</i>	25	1.965 2.006	1.966	<i>V5=1437</i>	1470	100%	900	Layer 5
<i>Q6=200</i> <i>100</i>	25	1.965 2.006	1.5	<i>V6=1437</i>	1500	100%	925	Layer 6
<i>Q7=200</i>	25	2.006 2.03	1.966	<i>V7=1470</i>	1430	50 %	950	Layer 7
<i>Q8=200</i>	25	2.03	1.5	<i>V8=1568</i>	1600	25 %	975	Layer 8
<i>Q9=200</i>	25	1.965	1.966	<i>V9=1430</i>	1430	25 %	1000	Layer 9
<i>Q10=200</i>	25	1.5	1.5	<i>V10=1568</i>	1600	25 %	1025	Layer 10
<i>Q11=200</i>	25	1.96	1.966	<i>V11=2500</i>	2500	25 %	1050	Layer 11

Table 3.b. Seismic model parameters large model

Background model

```

D = [80,560,80,155,25,25,25,25,25,25,25];
rho = [1.0,1.5,2.0,2.03,2.006,1.965,2.006,2.03,1.96,1.5,1.96];
v = [1480,1600,2000,1800,1470,1500,1430,1600,1430,1600,2500];
Q1 = [1000,1000,1000,1000,1000,1000,1000,1000,1000,1000,1000];
Q2 = [200,200,200,200,200,200,200,200,200,200,200];
    
```

% Depth [m]
 % density [g/cm3]
 % velocity [m/s]
 % absorption Q.

Saturated model

```

D = [80,560,80,155,25,25,25,25,25,25,25];
rho = [1.0,1.5,2.0,2.0,1.966,1.5,1.966,1.5,1.966,1.5,1.966];
v = [1480,1600,2000,1800,1470,1500,1430,1600,1430,1600,2500];
Q1 = [1000,1000,1000,1000,1000,1000,1000,1000,1000,1000,1000];
Q2 = [200,200,200,200,100,100,200,200,200,200,200];
    
```

% Depth [m]
 % density [g/cm3]
 % velocity [m/s]
 % absorption Q.
 % absorption Q.

The background model gives us the structure of the sediments without CO2. Different saturations with CO2 will give us different values for velocity and density (Table 2). This is called deviation from the background model (saturated model). Also absorption will change for different saturations (Fig.6) both

for table 3.a and b. I have given alternative values from background model in yellow color both on table 3.a. and b

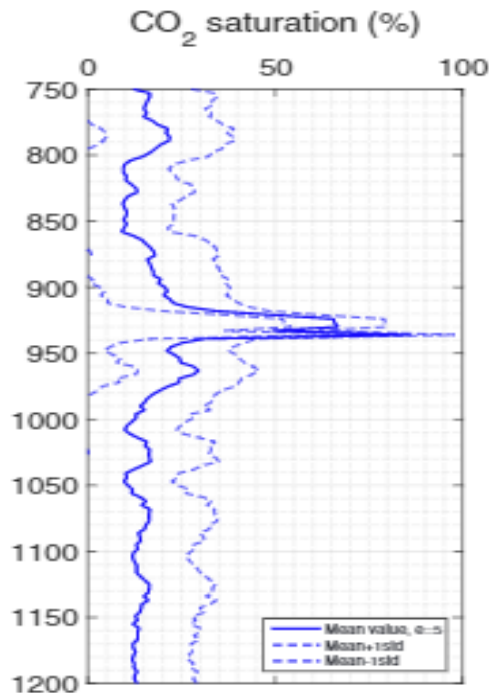


Figure 5. 1D profiles of CO₂-saturation estimation taken from Hong Yan (2018). The data is from Utsira sand, Sleipner field. Vertical axes is depth in meters. The CO₂-saturation is maximum (estimated 100%) between 900 and 950 meters (marked in table 3.b).

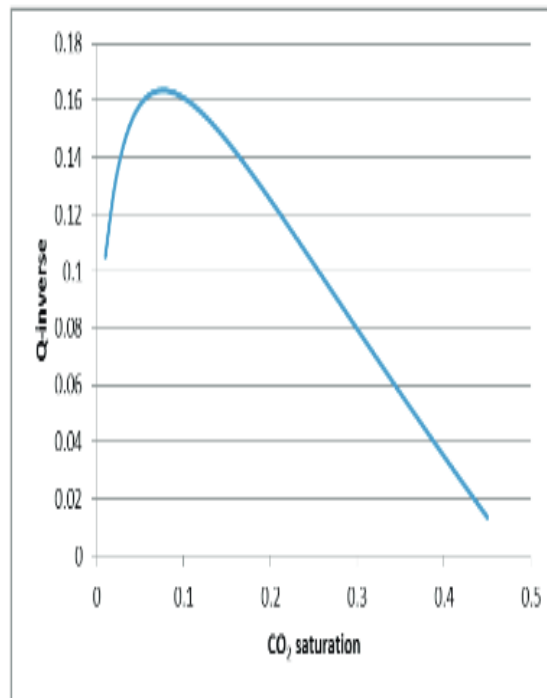


Figure 6 shows data of absorption. Hiroyuki Azuma (2014) .

I used some of the data from table 3 a. and b. for the synthetics. The tables are an attempt to include more accurate data for the section taking also the CO₂-saturation into account.

The free-surface-multiples were easily introduced and required a water layer (150 m in small model and 80m in large model) above the other layers as introduced in Eq.(22). Density of the water layer is 1 g/cm³ and velocity is 1480 km/h. The synthetics with free-surface multiples are graphs on fig.7.

With a background model without attenuation we achieved the synthetics with surface-multiples as the black trace on the left fig.7. Red graph in same plot is synthetics with interbed and without surface-multiples. Then we have cplot with both interbed and free-surface multiples. Free-surface multiples are dominant compared to interbeds. The reflectors are then introduced to the right for the cplot.

So, we introduced attenuation. We used $Q(1)=Q(2)=Q(3)=100$. We have used the absorptionmodel of Wang with $2\pi\omega_h=140$ Hz. The next plot to the right shows synthetics without attenuation (black) and with attenuation (red). Then to the right we have synthetics without free surface-multiples and with interbed multiples. Reflectors are easily visible on all plots (red circles).

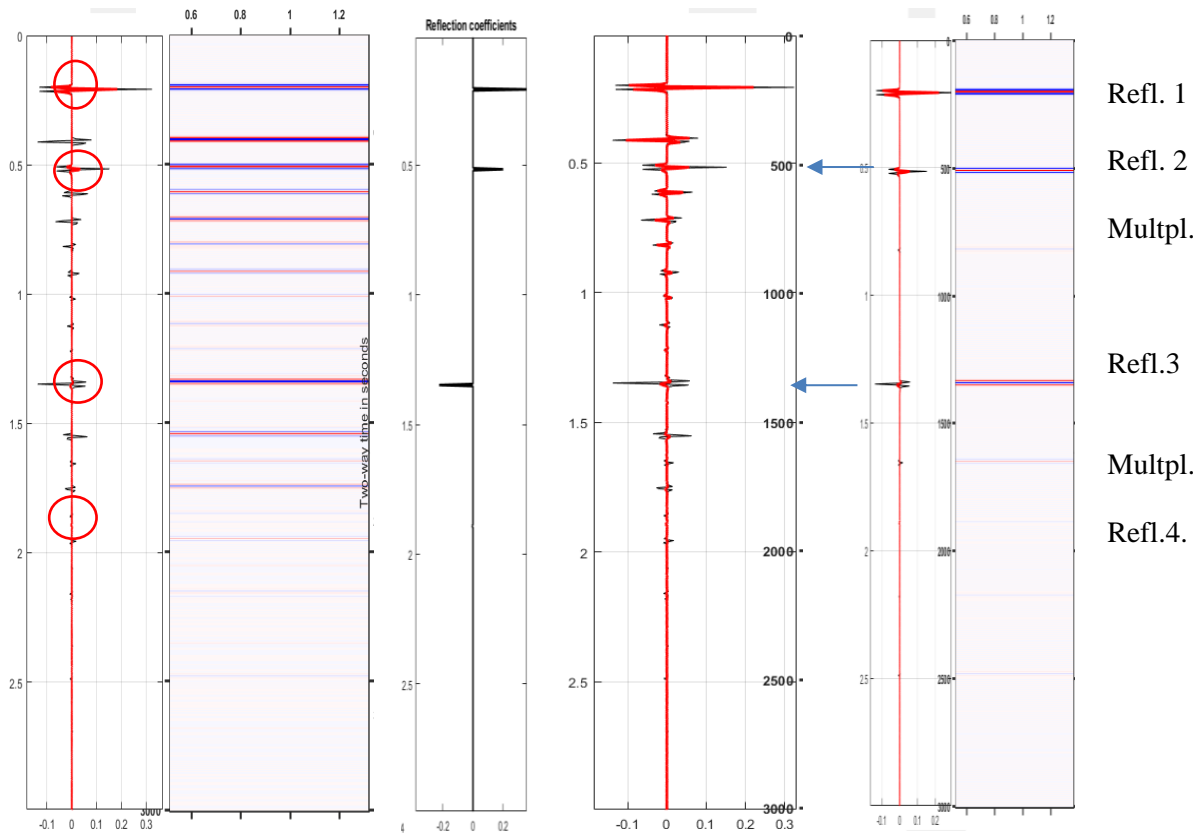


Fig. 7. We used $Q(1)=Q(2)=Q(3)=100$. We have used the absorption model of Wang with $\omega_h=2\pi 140$ Hz. The next plot to the right shows synthetics without attenuation (black) and with attenuation (red). Then to the right we have synthetics without free surface-multiples and with interbed multiples.

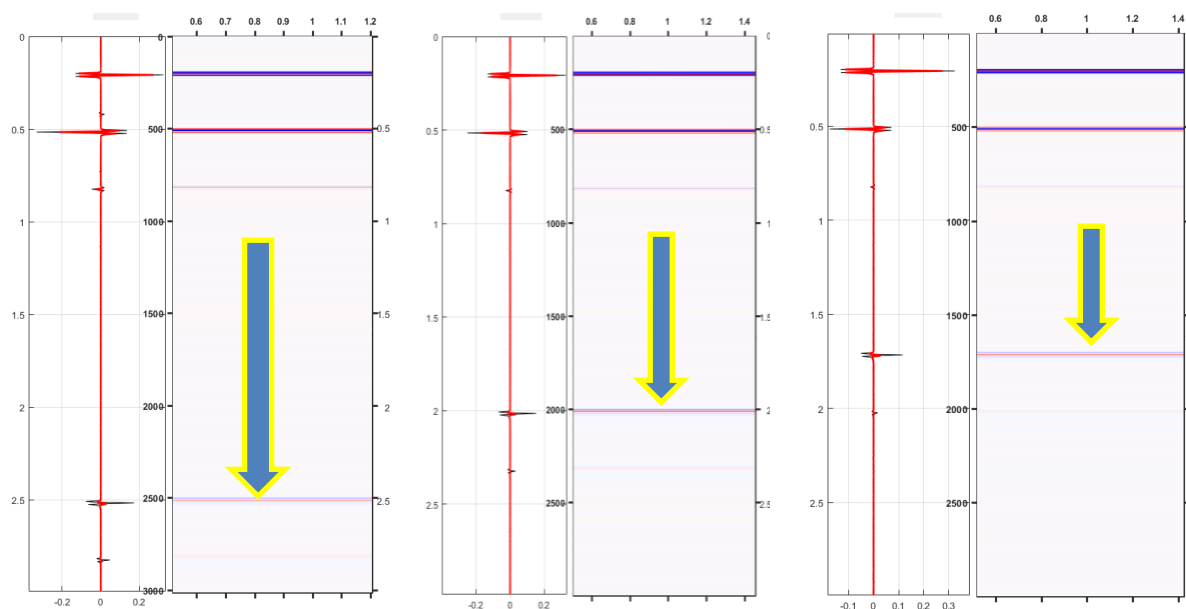


Figure 8. Layer 3/4 moves down with more CO2 saturation. More CO2 decrease velocity in the layer and reflector moves down (from right to left). Left is velocity $v= 600$, then $v=800$, and then $v=1000$

Figure 8 shows what happens when we introduce more CO2 into one of the layers. Decreasing velocity will move reflector 3 up in the layer. According to table 2 more CO2 in a layer will decrease velocity. Then the synthetics will show the layer more down in the sediments than in the case of the background model.

The opposite effect comes from absorption. According to Fig.6 more CO2 will decrease absorption and the reflector will be moved upwards. This is shown on fig.9

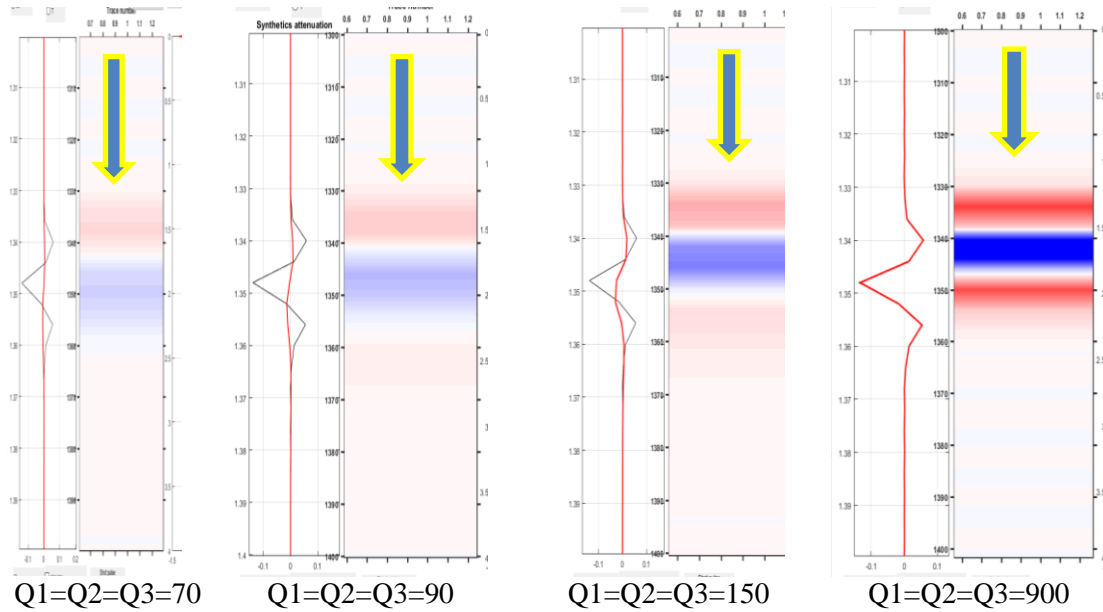


Figure 9. Absorption gives a result opposite of fig.8. More CO2 will decrease absorption (increase the quality factor Q) and the reflector moves upward. (from left to right). The reflector is more sharp with decreasing absorption.

From fig.7-9 we have a good reconstruction of the synthetics with parameters from table 3.a (small model) and we can conclude that the solution Eq. (17) gives us a good solution of the Riccati equation in the forward case (synthetics), when the effect of CO2 is taken into account..

Before we jump to the inversion, we need to give a remark about the impedance. The relation between r and the impedance makes it possible to compute the impedance for every solution of r . If the acoustic impedance I_0 is known at $z = 0$, (or at any depth), I is also uniquely determined as a function of τ . From Eq. (11) we can deduce:

$$I = I_0 \exp\left(2 \int_0^\tau r(\tau) d\tau\right) \tag{25}$$

where $I_0 = \rho_0 v_0$ and I/I_0 will give us a dimensionless relative impedance. We will come back to this in the next section.

Inversion LSQ – inverse numerical implementation

In the following we will implement the layered model parameters (Table 3.a and b) that was used to generate the synthetic seismograms in the forward modeling above. The inversion will be done taking the forward modelled synthetic seismograms as input. The procedure will be done with a conventional least square (LSQ) seismic inversion procedure. We will see that an LSQ-inversion is all we need to recover the reflection coefficients from the synthetics .

Consider Eq. (17) in the limit $\tau \rightarrow 0$, which gives the ‘seismogram’

$$K(\omega, 0) = \int_0^T r(\tau') \exp(-\phi(\omega, \tau')) (1 - K^2(\omega, \tau')) d\tau' \quad (26)$$

Introduce ‘reflectivity’ series

$$r(\tau) = \Delta\tau \sum_{i=0}^{NT-1} r_i \delta(\tau - i\Delta\tau), T = NT \cdot \Delta\tau \quad (27)$$

Combination of Eqs. (26) and (27) gives

$$K(\omega, 0) = \sum_{i=0}^{NT-1} r_i \exp(-\phi(\omega, i\Delta\tau)) (1 - K^2(\omega, i\Delta\tau)) \Delta\tau \quad (28)$$

Originally, seismogram recorded in timedomain, i.e. $k(t, 0)$, and assume sampled with a total of NT -samples. Fourier transform of the data will give the same number of monochromatic seismograms.

Nilsen and Gjevik introduced an iterative inversion procedure to solve for r in eq.(26) when the reflection response of the reflecting layer is known. When absorption was included that could be a complicated process and as far as we know no calculations were done with absorption by them.

Leiv Gelius, in an unpublished note, suggested a more elegant solution of the equation with the matrix system:

$$\begin{bmatrix} K_{n+1}(\omega_0, 0) \\ K_{n+1}(\omega_1, 0) \\ \cdot \\ \cdot \\ K_{n+1}(\omega_{NT-1}, 0) \end{bmatrix} = \quad (29)$$

$$\begin{pmatrix} \exp(-\phi(\omega_0, 0)(1 - K_{0,n}^2) & \exp(-\phi(\omega_0, \Delta\tau)(1 - K_{1,n}^2) & \dots & \exp(-\phi(\omega_0, (NT-1)\Delta\tau)(1 - K_{n,n}^2) \\ \exp(-\phi(\omega_1, 0)(1 - K_{0,n}^2) & \exp(-\phi(\omega_1, \Delta\tau)(1 - K_{1,n}^2) & \dots & \exp(-\phi(\omega_1, (NT-1)\Delta\tau)(1 - K_{n,n}^2) \\ \cdot & \cdot & \dots & \cdot \\ \cdot & \cdot & \dots & \cdot \\ \cdot & \cdot & \dots & \cdot \\ \exp(-\phi(\omega_{NT-1}, 0)(1 - K_{0,n}^2) & \exp(-\phi(\omega_{NT-1}, \Delta\tau)(1 - K_{1,n}^2) & \dots & \exp(-\phi(\omega_{NT-1}, (NT-1)\Delta\tau)(1 - K_{n,n}^2) \end{pmatrix} \begin{pmatrix} r_{n,0} \\ r_{n,1} \\ \cdot \\ \cdot \\ r_{n,NT-1} \end{pmatrix}$$

Hagos (2016) made some computations for Eq.(29) in his thesis. A more detailed study of the solution is in appendix 2. The mathematics for how to do least square inversion is also outlined in Sørdsdal (2018).

Note that $K_0^2=0$ in the first iteration. After a new estimate of the reflectivity series has been obtained, an update of $K_{i,n}^2$ can be obtained by solving the forward problem. Iterations are carried out until the relative change in reflectivity is below a certain user threshold. The effect of the inversion when $K^2 = 0$ is simply to compensate for the damping of the amplitude caused by attenuation and correct the phase term caused by dispersion. When $K^2 \neq 0$ we also remove multiples and compensate transmission loss. Surface multiples can also be removed simply by multiplying K with the inverse of RHS of Eq (22). First we remove surface multiples before we solve Eq.(29). This can simply be done multiplying r with the inverse of Eq. (22)

Fig.10 shows the inversion of Eq.(29) with the synthetics r as input. I took the second plot from left on fig.9 as input. The inversion (middle plot) gives us a sharp layer (blue). Right plot from middle plot shows the impedance and then the reflector model.

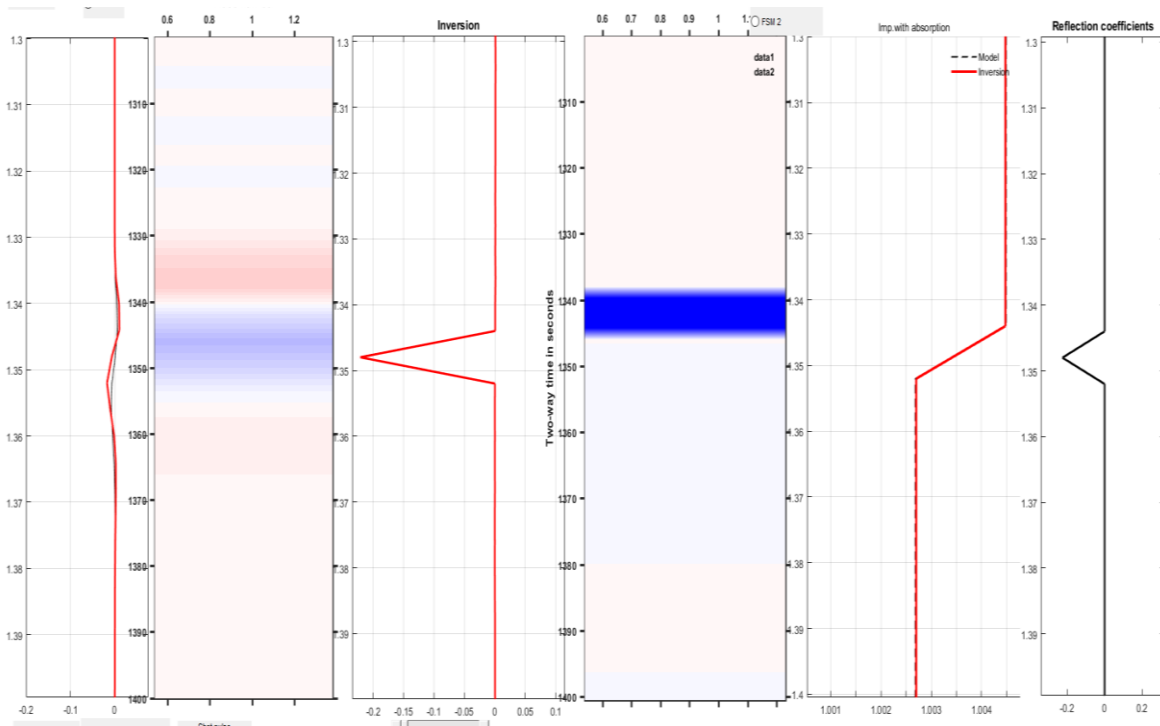


Figure 10. From fig.9 (synthetics) with $Q=90$ we did an LSQ-inversion. We achieved a sharp spike reflector. (middle plot). Next plot is I (Eq.(25)).

Fig.11.a-d shows solutions for the complete model with parameters from table 3.a. for different values. We have no free surface multiples. Change in velocity will have an effect as well as the effect of change in Q -value but it depends on the value. Decrease in velocity will delay the seismic signal and the layer will appear to be deeper in the ground as on fig.11.a..

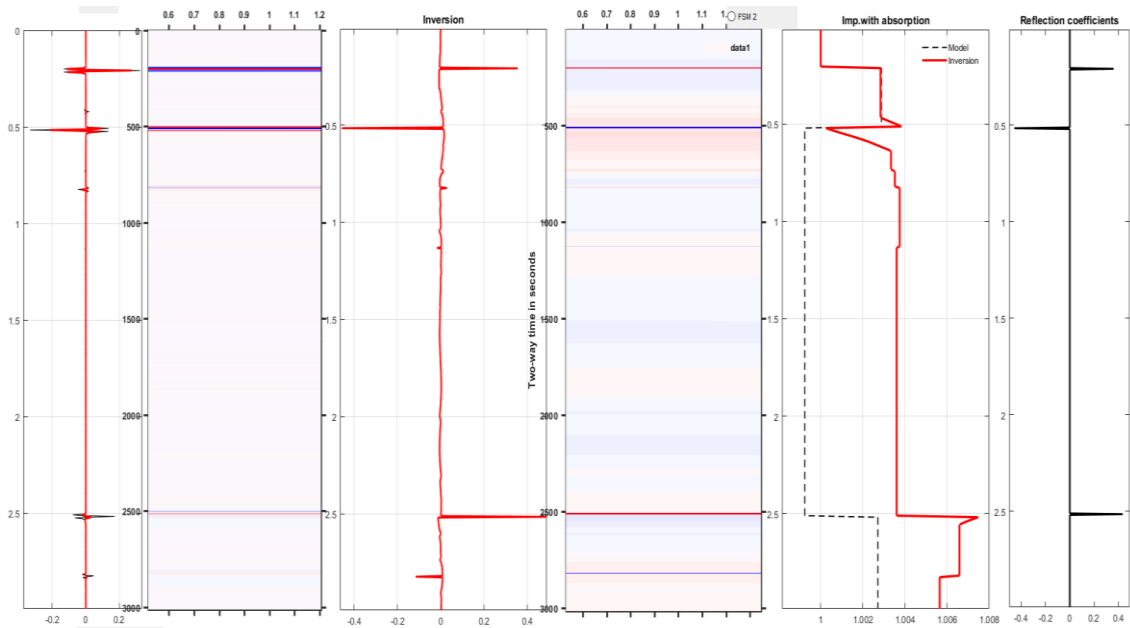


Figure 11.a Synthetics – trace and cplot - (from left) and then inversion – trace and cplot - with data from Table 3.a.. Then impedance inversion – black dots model, red inversion trace. Right plot is the reflectors. $V=600$ m/s, $Q=200$ for all layers

More absorption (lower Q-value) will have the same effect. This could be seen from the phase velocity fig.3, but on fig.11.a. absorption is too low to have an effect on the synthetics. Both absorption and low velocity delays the signal. (Remember that more CO₂-saturation gives less absorption than high, so as a function of CO₂-saturation absorption will decrease). Both effects is a consequence of CO₂-saturation. If the signal from CO₂-layer will be abruptly changed due to low velocity, however, it can also result in high reflectors that could make problems for the inversion. We could, in that case, expect more interbed multiples. Both figure 11.a. and b. show interbeds and the impedance inversions shows difference between model (black dotted) and inversion (red).

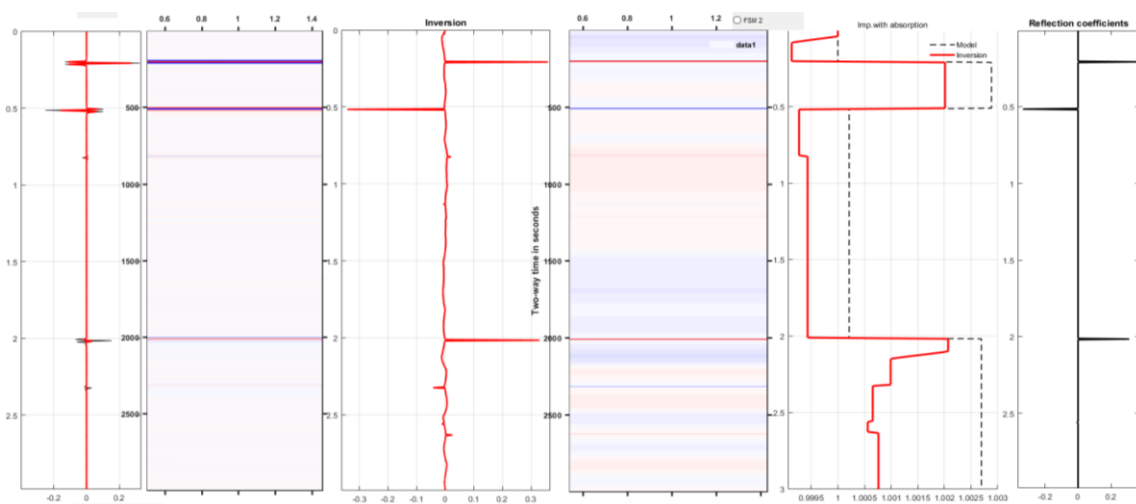


Figure 11.b Synthetics – trace and cplot - (from left) and then inversion – trace and cplot - with data from Table 3.a.. Then impedance inversion – black dots model, red inversion trace. Right plot is the reflectors. $V=800$ m/s

Trying higher velocity (1000 m/s) on fig.11.c we got a better inversion. Impedance model (black dotted graph) is close to the impedance inversion (red graph). For lower reflectors, creating less interbeds, the inversion goes better than for higher velocities.

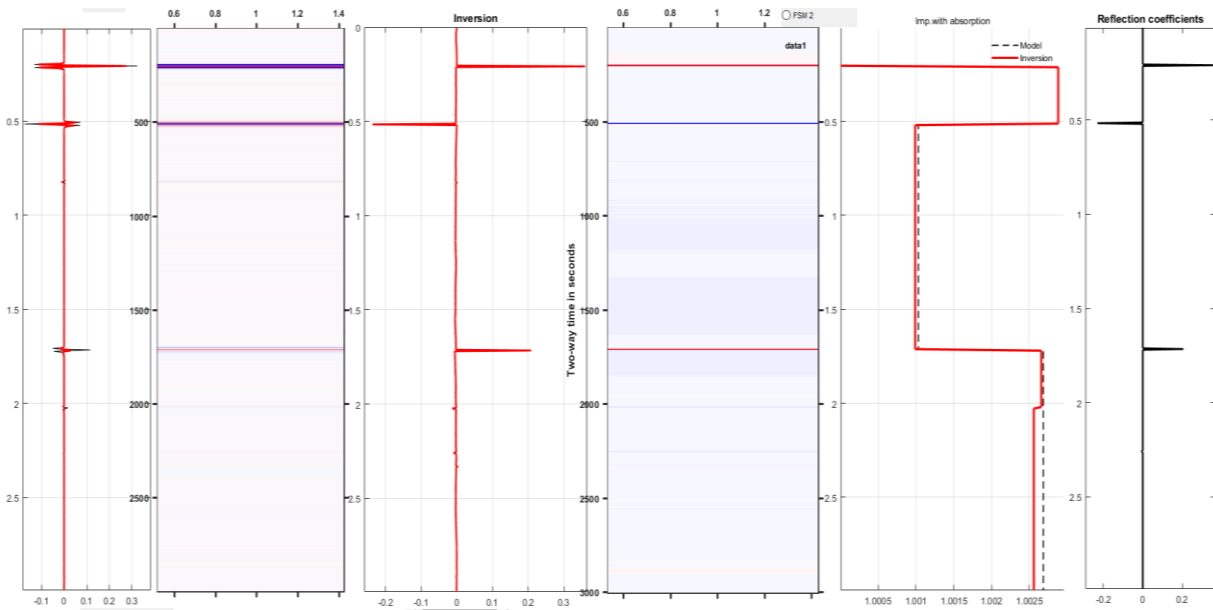


Figure 11.c Synthetics – trace and cplot - (from left) and then inversion – trace and cplot - with data from Table 3.a.. Then impedance inversion – black dots model, red inversion trace. Right plot is the reflectors. $V_3=1000$ m/s

We can state that from table 2 more CO₂-saturation will give lower velocities in the layer 3 and move the layer down on the seismogram, and from fig.6. we can state that absorption could move the layer up again. But since more CO₂ in the layer will give less absorption, we will choose the model with very high velocity in layer 3 to test the effect of absorption.

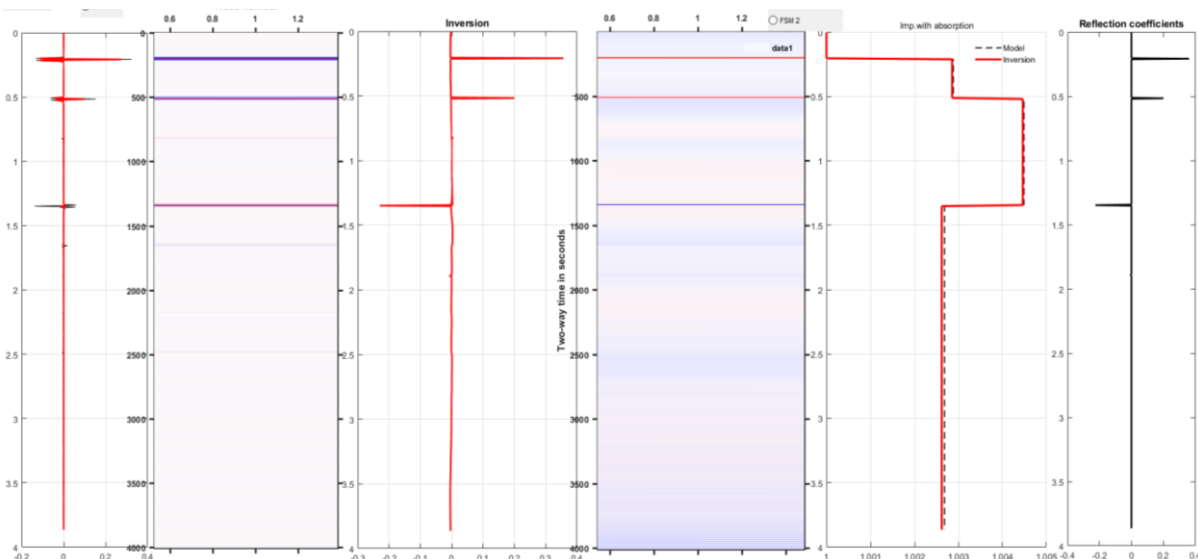
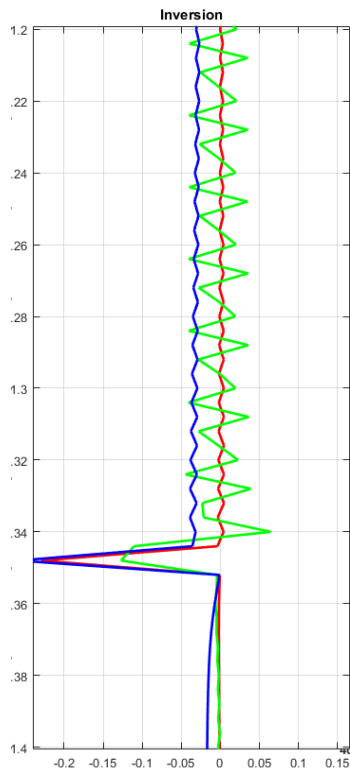


Figure 11.d Synthetics – trace and cplot - (from left) and then inversion – trace and cplot - with data from Table 3.a.. Then impedance inversion – black dots model, red inversion trace. Right plot is the reflectors. $V_3=2400$ m/s, $Q_3=100$



We have high velocity $v_3=2400$ m/s and with absorption $Q_1=Q_2=200$, and $Q_3=100$ we got a fairly good inversion on fig.12. (red graph). Changing to $Q_3=70$ we got more noise into the inversion (green graph). However, we can clearly see that the reflector is moved up in comparison to the solution with $Q_3=100$. However, for our Q-values this is very small compared to the effect from lower velocity. Blue graph is an attempt with $Q_3=80$. This is very close to the model.

Figure 12. Inversion of the third reflector with parameters based on table 3.a. Blue graph with $Q_3=80$ is very close to the model with $Q_3=100$.

We can see clearly from fig.12 that absorption will move the reflector upwards, and more absorption is actual when CO2-saturation is low. Therefore, when we have much CO2 in the model we must expect that the reflectors will move downwards. The effect from low velocity is considerably stronger than the opposite effect from absorption.

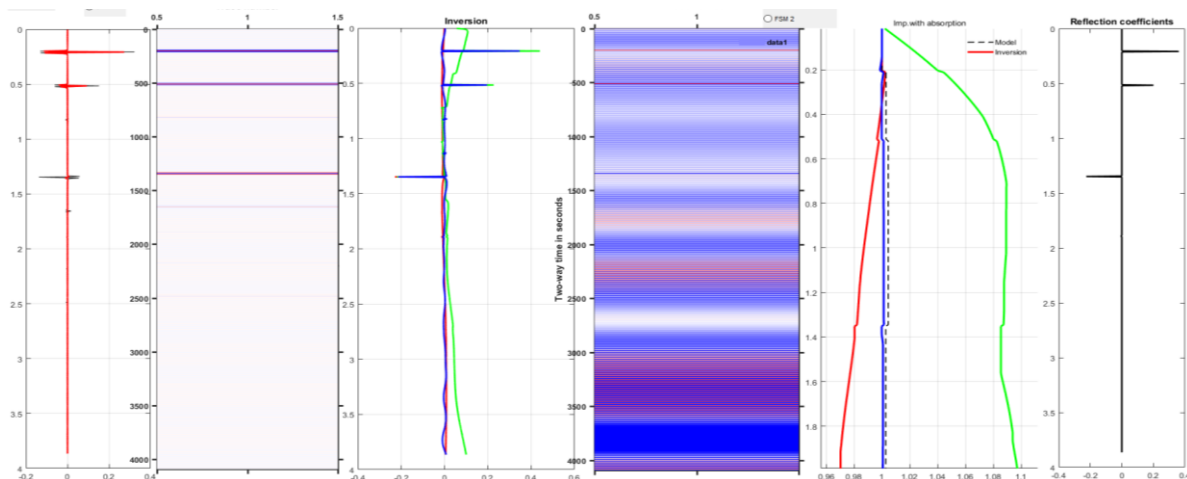


Figure 13.a. Synthetics – trace and cplot - (from left) and then inversion – trace and cplot - with data from Table 3.a.. Then impedance inversion – black dots model, red inversion trace. Right plot is the reflectors. $V=2400$ m/s, $Q_2=180$, $Q_3=80$ (blue), $Q_2=170$ (red), $Q_1=160$

We must realize that the inversion is very sensitive to absorption. Figure 13.a. blue graph (inversion and impedance inversion) is a solution with $Q_2=180$, $Q_3=80$ and $v=1000$ m/s is closest to the model. (black dotted). The cplot has much noise.

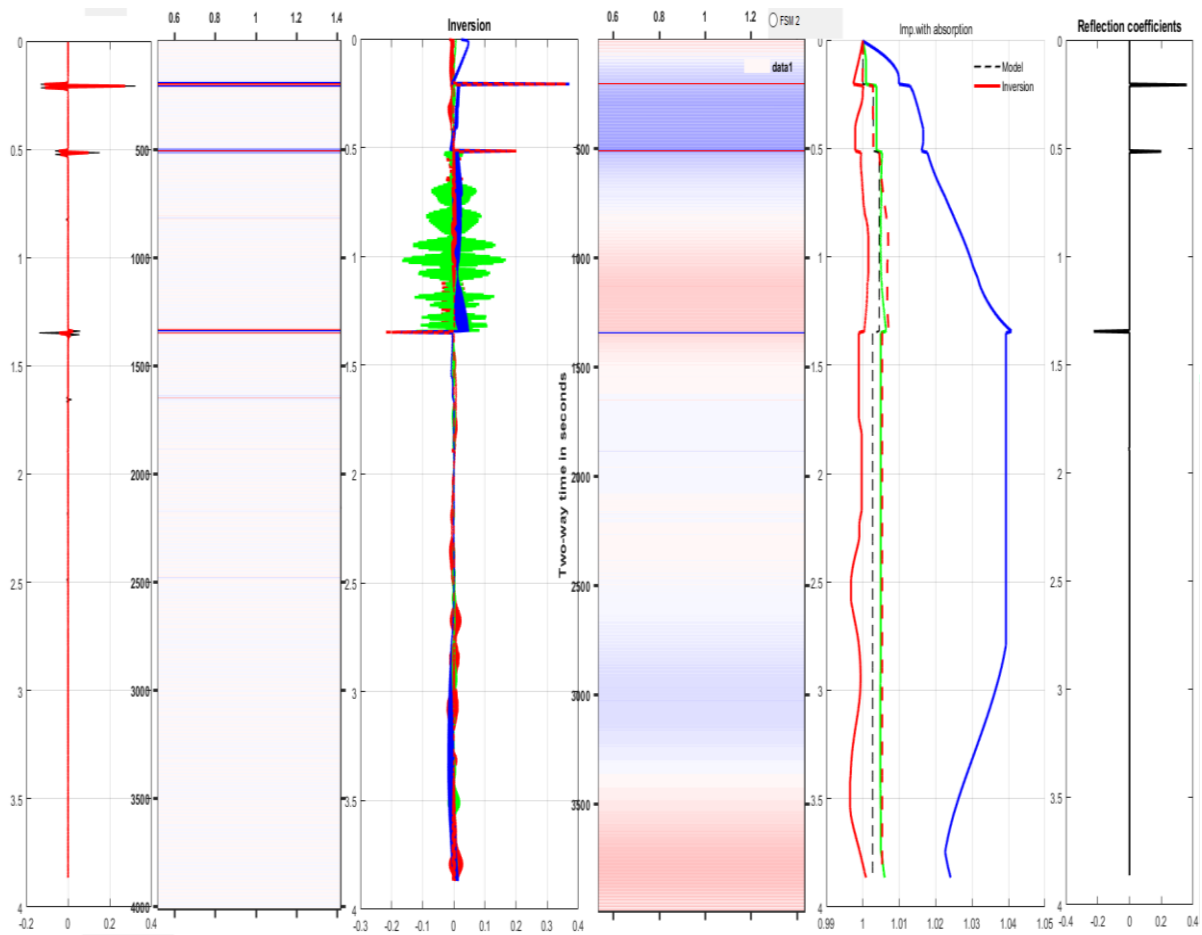


Fig.13.b. Red: $Q_2=200, Q_3=70$, blue: $Q_3=100$, green: $Q_3=170$ red dots: $Q_3=200 v_3=2400$

Green graph is very close to the model. And it is not so much noise in cplot in fig.13.b. as in fig.13.a.

So, to sum up: the solution to Eq.(29) after inversion will be important for further study. The idea of the inversion is to compare the impedance from the seismic model with the impedance after the inversion. The success of the inversion depends on how close the impedance we compute from the inverted data are to the impedance from the model data.

Fig.11. a,b,c and d shows a solution r after 5 iterations, and with parameters from table 3.a. respectively. Surface multiples are removed simply by multiplying r with the inverse of Eq. (22) but in this plot we did not implement free surface-multiples. Then in further iterations interbed multiples are removed so interbeds are removed in the final solution.

The impedance-inversion (5.th. graph from left) gives a good picture of the inversion. Direct from the reflectors we can calculate an impedance we call the reflector-model impedance (black dotted). Graphs indistinguishable from (or close to) black dotted graph shows 5. iteration plotted on the model gives us a good inversion. The shot pulse were removed and absorption restored in the final solution.

Fig.14.a. gave us a good inversion of the background model with data from table 3.b removing, interbed multiples and restoring transmission loss. The background model is model of the sediments without CO2.

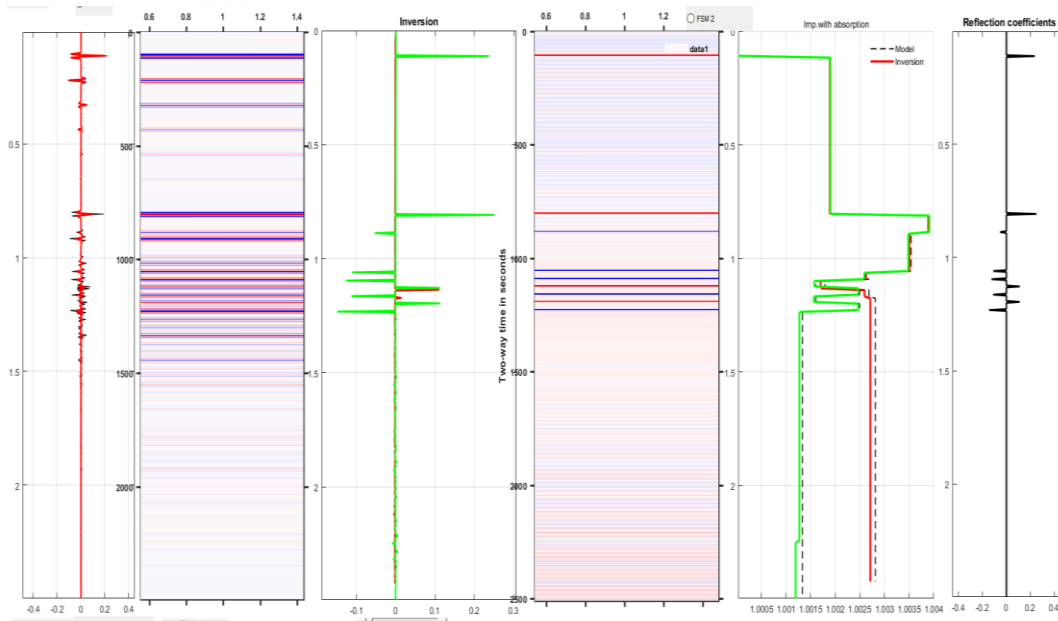


Fig.14.a. Data from table 3.b. From left: Synthetics with all multiples. Then synthetics cplot. Then full background inversion , and then cplot inversion. Background impedance inversion is close to the model. (black dotted). Right plot: reflection coefficients for the model. $V_3=2400$ m/s.

Now to the CO2-saturated model. CO2 will give lower density and slower velocity than the background model. Highly saturated model will give lower attenuation than less saturated (maximum at 10 % CO2 saturation).

Fig.14.b gives an inversion of the saturated model for different parameters. Fig.14.b. deviates from fig.14.a. simply by a change of absorption from $Q_3=200$ to $Q_3=100$.

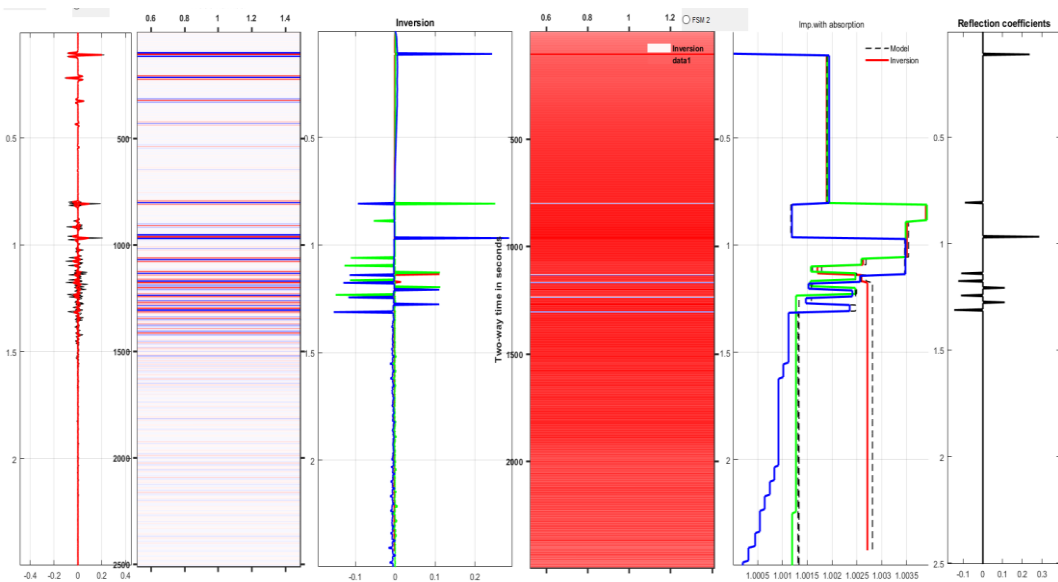


Fig.14.b. Data from table 3 (CO2 saturated). From left: Synthetics with all multiples). Then synthetics cplot. Then full CO2-saturated inversion and then cplot inversion. Then impedance inversion, and Reflector model is to the right. green : $V_3=2400, Q_3=100$, blue : $V_3=1000, Q_3=100$, red: $Q_3=100, V_3=2400$ m/s.

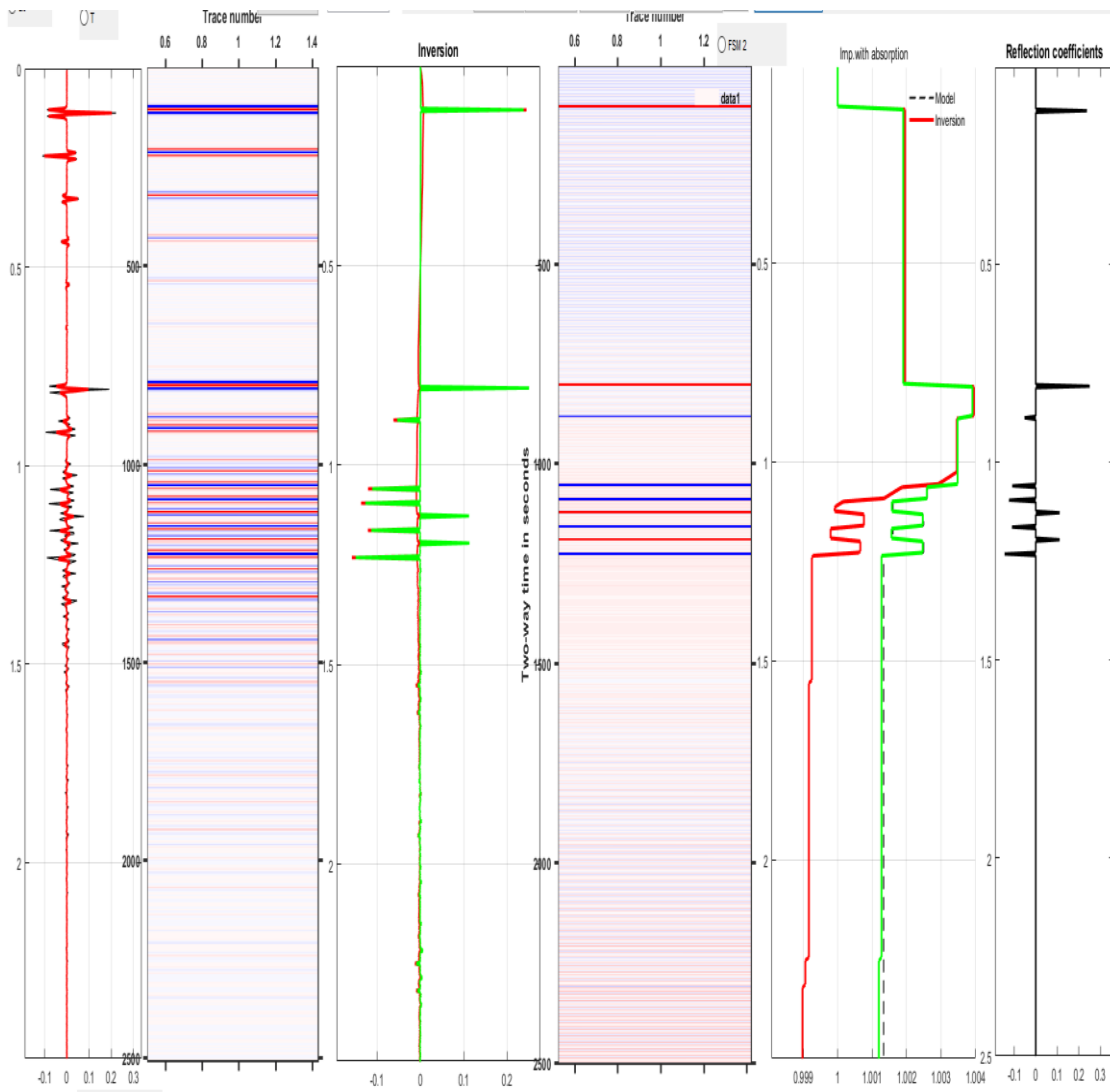


Fig.15.a Data from Table 3.b. green : $V_3=2400, Q_3=100$, Absorption is changed to red: $Q_3=100, V_3=2000$ m/s

Fig.15 a. is the background model with data from Table 3.b. (green graph). Red graph is saturated model from Table 3.b with a small modification. Velocity through layer 3 is changed from $v=2400$ m/s to $v=2000$ m/s. The reason for this is that this velocity made the CO2 saturated model more close to the reflector-model. (dotted line).

It is important to notice that the lag between the background model and the CO2-saturated model is due to slower velocity in the saturated model. The absorption will also give some dispersion, but slower velocity will dominate. We will be able to see this, knowing that all dispersion caused by viscoelasticity is corrected for in the LSQ-inversion. I have documented this in previous articles Sørdsdal (2018) and Sørdsdal (2019). The velocity change, however, is not corrected for in the inversion of the saturated model. I will come back to this in a later article.

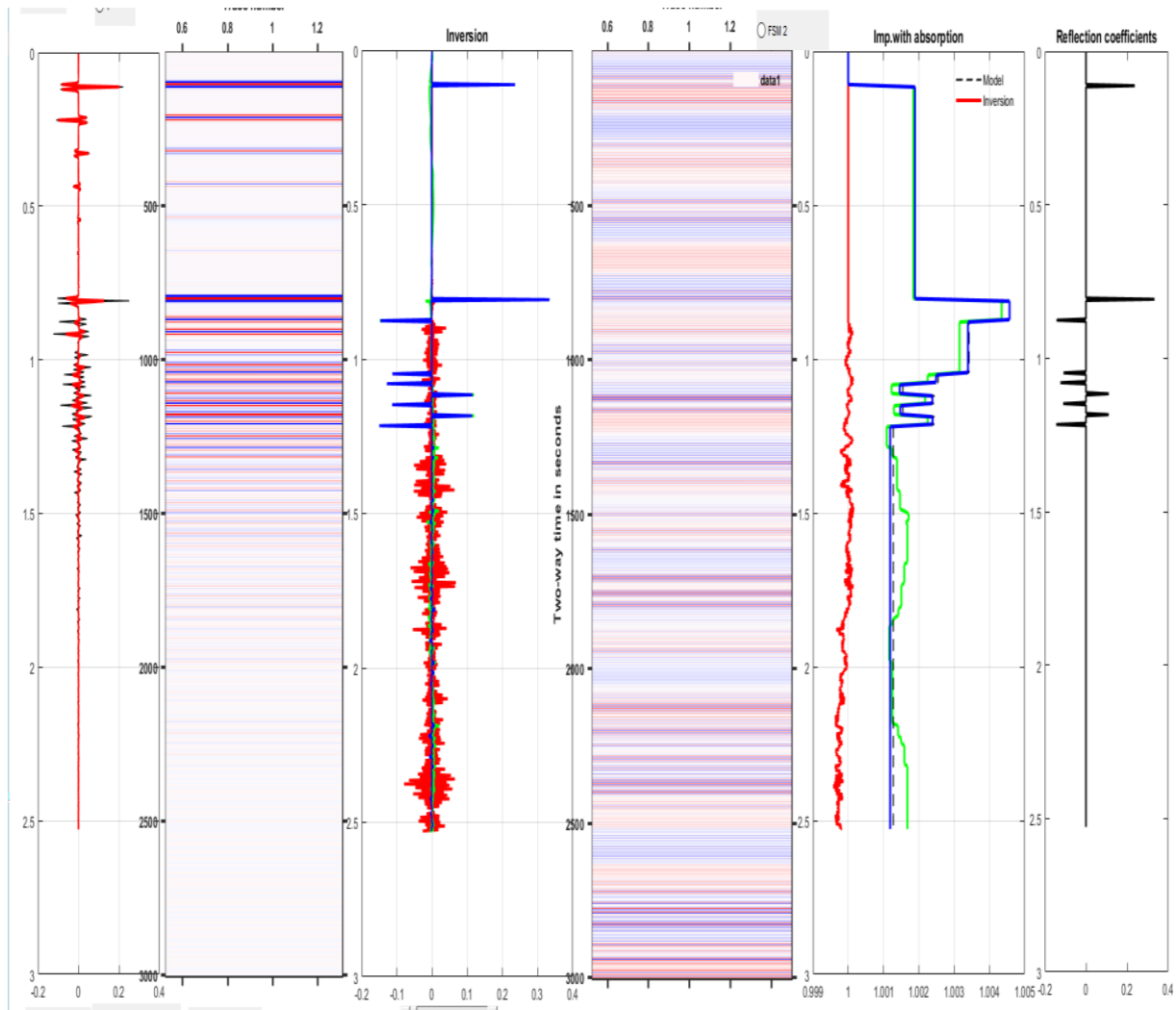


Fig.15.b red $Q_3=70$, green $Q_3=80$, blue $Q_3=100$ $v_3=2400$ cplot with $Q_3=80$, free surface multiples in synth.

On fig.15 b we see saturated CO2 model for different Q-values. Left plot is synthetics with all multiples. Then cplot of synthetics and the inversion. Next cplot is inversion with $Q=70$. It deviates much from the cplot of synthetics. Problems with inversion for high absorption green $Q=80$, blue $Q=90$ red $Q=70$. Inversion with $Q_3=100$ gave a good inversion with cplot as on fig. 15.a.

Fig.15.c gives us the same data as fig.15.b. However, cplot of the inversion gave us a solution similar to the cplot of fig.15.a. we can conclude that we get a good inversion as long as the absorption Q is 80 or higher.

To sum up, we got a very good solution with LSQ, indistinguishable from the model for our impedance models (Table 3.a. and b). The inclusion of surface multiples were very well implemented, but not important for our theory, since we removed them before using LSQ. All the other effects, however, are important for the LSQ-solution. All features are introduced by 5 iterations of the synthetics, attenuation and dispersion included and was removed or restored in the inversion.

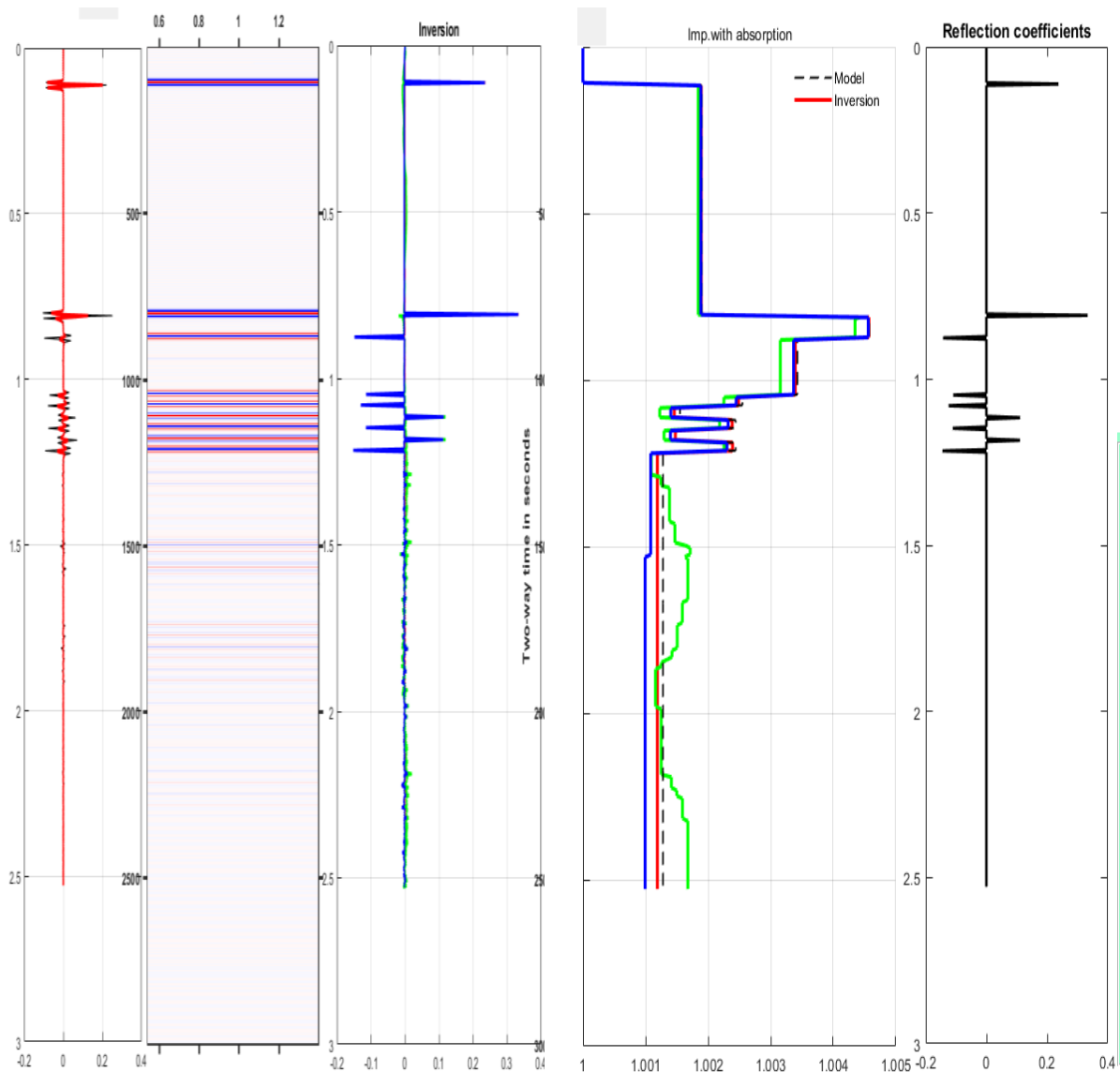


Fig.15.c green $Q=80$, red $Q=100$ $v_3=2400$, no free surface multiples cplot with $Q=80$

So, to further sum up, 5 forward iterations gave us the synthetics. Then we use synthetics as input counting K^2 zero and computing the first LSQ-solution for K . Now we put this K into Eq. (29). and get a new iterated inversion. We repeat this 5 times. Then we see that interbed multiples are removed and transmission loss and attenuation are restored as well as shot pulse removed. Dispersion is also compensated for. However, attenuation is not so good restored for with $Q < 80$. Fig.15 a and b shows the calculations with $Q=70$ and with higher Q -values. Impedance inversions shows a solution very different from the background model, and we can expect problems studying inversion with high attenuation.

A closer look at the inversion

Ultimately, after the development of the previous theory we have been able to combine a forward solution of Kolsky-Wang Q -filter with a LSQ-solution for inversion. So we have fulfilled the purpose of this article. However, a broader view of the subject could be interesting in the future and a further study of Q -filtering is necessary..

So, to even further sum up: setting $K^2=0$ in eq (29) we achieved the linear solution on matrix form and solved this for r as a time-domain vector that represents the filter. The inverse Q-filtering procedure was performed successively to each time sample to get the time-dominant output vector. We then used the output r as input getting the inverted solution for a new inverted r . When we do this we can, of course, replace the Q-filters with the inverse Q-filters as Wang did, and this could be a further study. Then we also will need to study the stabilization of the inverse filter, gain limitation and so on. However, the LSQ-solution in this paper simplified the study. A more complicated theory for the LSQ-solution are introduced in appendix 2. It is called the regularization of the LSQ-solution. It was not necessary to introduce regularization in this study, to achieve the goal of the paper, but could be a subject for further study.

Further iterations in the Riccati-solution introduced non-linearity on the way to a seismic theory that can be used on real data and will be, as far as I can see, a broader and better theory than the theory of Wang that was strictly linear. And, of course, the application of the theory applied on CO₂-monitoring is more relevant in today's world than traditional seismic for oil prospecting.

Conclusion

The results of the preceding sections show that the Riccati equation with Q-filtering provides a method for the construction of synthetic reflection seismograms that is a continuation of the method introduced by Nilsen and Gjevik. Moreover does this theory describe a method for inverting reflection data, i.e. computing the variations in the acoustic impedance within a reflecting layer that can be used in real prospecting. This I have briefly suggested by introducing a water layer over a very simple seismic model and a more complicated seismic model from the Sleipner field. And the Riccati inversion corrects phase, compensates frequency loss, removes multiples and compensates transmission loss in one single process.

In my previous articles I tested the abilities of the inversion method by inverting a synthetic reflection seismograms computed from a simple impedance model with a water layer. And frankly, this article does not introduce so much more that concern real seismic prospecting. It would, however – as Gjevik suggested several years ago - be interesting to apply the present inversion method to real reflection data from a more complex structure. A number of problems will then arise as was discussed in the paper of Nilsen and Gjevik. However, because of years of rapid development in inversion theory, this is much easier solved today than when the theory first was introduced.

Even if this could be done only with a limited degree of accuracy, the main problem is, however, that what Gjevik asked is not fully answered: will one lose so much information or introduce so many errors through this process that the inversion becomes meaningless when applied to real prospecting? In view of the success of the application on data from the Sleipner field this question could soon be answered.

References

- Gjevik et al. (1976) *An attempt at the inversion of reflection data. Geophysical prospecting* 24,492-505
- Nilsen and Gjevik (1978): *Inversion of reflection data. Geophysical prospecting* 26, 421-432
- Yanghua Wang (2008) *Blackwell Publishing. Seismic inverse Q filtering*

Knut Sørdsdal (1981) Viskoelastiske dempningsmodeller i Riccatiligningen anvendt i marin seismikk. University of Oslo

Knut Sørdsdal (2019) Seismic Q-filter models applied to the Riccati equation
https://www.researchgate.net/publication/337682839_Seismic_Q-filter_models_applied_to_the_Riccati_equation

Knut Sørdsdal (2018) 1-D non-linear inversion of data with absorption - revisited.
https://www.researchgate.net/publication/331257025_1-D_non-linear_inversion_of_data_with_absorption_-_revisited

Bland(1960) The theory of linear viscoelasticity. Pergamon Press

Horton (1959) A loss mechanism for the Pierre Shale. Geophysics vol.24, no 4

Aki and Richards (2002) Quantitative Seismology W.H. Freeman and Co. San Fransisco

Kolsky, 1956 The propagation of stress pulses in viscoelastic solids. Philosophical Magazine 1, 693-710

Kjartansson E. 1979 Constant Q wave propagation and attenuation. Journal of Geophysical Research 84 4737-48.

Futterman W.I 1962 Dispersive body waves. Journal of Geophysical Research 67 , 5279-91

Trorey A.W, 1962 Theoretical seismograms with frequency and depth dependent absorption. Geophysics 27, 766-85

Claerbout J.F.1976 Fundamentals of Geophysical Data Processing. McGraw-Hill Book Co. New York

Hagos Geberehiwet Gebregergs (2016): Compensation of Absorption Effects in Seismic Data. University of Oslo

Hong Yan, Bastien Dupuy, Anouar Romdhane and Børge Arntsen
Geophysical Prospecting, 2019, 67, 1055–1071 CO₂ saturation estimates at Sleipner (North Sea) from seismic tomography and rock physics inversion

Janita Louise Nordahl : (2015) Modeling of seismic amplitude anomalies associated with CO₂ underground storage — EOM-3901 Master's Thesis in Energy, Climate and Environment

KARSTENS, J. & BERNDT, C. 2015. Seismic chimneys in the Southern Viking Graben – Implications for palaeo fluid migration and overpressure evolution. Earth and Planetary Science Letters, 412, 88-100.

HALLAND, E. K., JOHANSEN, W. T. & RIIS, F. 2011. CO₂ Storage Atlas Norwegian North Sea, Norwegian Petroleum Directorate.

ARTS, R., EIKEN, O., CHADWICK, A., ZWEIGEL, P., VAN DER MEER, B. & KIRBY, G. 2004a. Seismic monitoring at the Sleipner underground CO₂ storage site (North Sea). Geological Society, London, Special Publications, 233, 181-191.

ARTS, R., EIKEN, O., CHADWICK, A., ZWEIGEL, P., VAN DER MEER, L. & ZINSZNER, B. 2004b. Monitoring of CO2 injected at Sleipner using time-lapse seismic data. *Energy*, 29, 1383-1392.

Hiroiyuki Azuma (2014) Utilization of seismic attenuation in the monitoring of CO2 geological storage project. *Science Direct*.

Appendix 1

In the literature the wavenumber k is often written on the following form in case of absorption (constant-Q model)

$$k = \frac{\omega}{v(\omega)} \left[1 - \frac{i}{2Q} \right] = \frac{\omega}{v_r} + \left[\frac{\omega}{v(\omega)} - \frac{\omega}{v_r} \right] - i\alpha(\omega) = \frac{\omega}{v_r} + \varphi(\omega) - i\alpha(\omega). \quad \alpha = \frac{\omega}{2Qv(\omega)} \quad (\text{A.1})$$

Where α is the absorption coefficient and φ is the phase of the ‘absorption filter’. In order to ensure causality, the filter should be minimum phase. For such a filter this relationship holds.

$$\varphi(\omega) = \text{H} [\alpha(\omega)]$$

With H denoting the Hilbert Transform. In case of no dispersion ($\varphi=0$), the filter will be noncausal. Then we have

$$k = \frac{\omega}{v_r \sqrt{Y}} = \frac{\omega}{v_r \sqrt{A + iB}} = \frac{\omega}{v_r} \left[\frac{1}{\sqrt{A}} - \frac{i}{2} \frac{B}{A\sqrt{A}} \right] \quad (\text{A.2})$$

Equating Eqs. (A.1) and (A.2) gives the relationships

$$A = \left[\frac{v(\omega)}{v_r} \right]^2 \quad B = \left[\frac{v(\omega)}{v_r} \right]^2 \frac{1}{Q}, \quad (\text{A.3})$$

Aki and Richards (2002) show that the following relation should be held to honor causality

$$\frac{\omega}{v(\omega)} - \frac{\omega}{v_\infty} = \text{H} \left[\frac{\omega}{2Qv_\infty} \right] \quad (\text{A.4})$$

Where v_∞ is the limit of the velocity function when ω tends to infinity. Equation (12) can be further approximated as

$$\frac{\omega}{v(\omega)} - \frac{\omega}{v_h} \cong \text{H} \left[\frac{\omega}{2Qv_\infty} \right] \quad (\text{A.5})$$

Where v_h is the velocity related to the highest possible (tuning) frequency of the seismic band. The wavenumber is accordingly adjusted as (compare with Eq.(A.1)).

$$k = \frac{\omega}{v_h} + \left[\frac{\omega}{v(\omega)} - \frac{\omega}{v_h} \right] - i \frac{\omega}{2Qv(\omega)} = \frac{\omega}{v_h} \left\{ 1 + \left[\frac{v_h}{v(\omega)} - 1 \right] - i \frac{v_h}{2Qv(\omega)} \right\} \quad (\text{A.6})$$

And combined with a Kolsky type of phase-velocity model (Kolsky, 1956)

$$v(\omega) = v_h \left(\frac{\omega}{\omega_h} \right)^\gamma, \quad \gamma = (\pi Q)^{-1} \quad (\text{A.7})$$

Gives the wavenumber model

$$k = \frac{\omega}{v_h} \left[1 + \left[\left(\frac{\omega}{\omega_h} \right)^{-\gamma} - 1 \right] - \frac{i}{2Q} \left(\frac{\omega}{\omega_h} \right)^{-\gamma} \right] \quad (\text{A.8})$$

Which has been employed by Wang. From Eqs. (A.1) and (A.2) it also follows that ($v_r = v_h$)

$$A_{Wang} = \left[\frac{\omega}{\omega_h} \right]^{2\gamma} B_{Wang} = \left[\frac{\omega}{\omega_h} \right]^{2\gamma} \frac{1}{Q} \quad (\text{A.9})$$

From Eq.(A.9) it follows that $0 < A_{Wang} < 1$, and the same for B_{Wang} but with $B_{Wang} \ll A_{Wang}$.

Based on Eq. (A.3), Kjartansson (1979) proposed an alternative wavenumber model

$$k = \frac{\omega}{v_\infty} + \left[\frac{\omega}{v(\omega)} - \frac{\omega}{v_\infty} \right] - i \frac{\omega}{2Qv_\infty} = \frac{\omega}{v_\infty} + H \left[\frac{\omega}{2Qv_\infty} \right] - i \frac{\omega}{2Qv_\infty} \quad (\text{A.10})$$

From Eqs.(11) and (A.10) it follows that ($v_r = v_\infty$)

$$A_{Futt} = \left[1 + \frac{1}{\omega} H \left(\frac{\omega}{2Q} \right) \right]^{-2} B_{Futt} = (A_{Futt})^{3/2} \frac{1}{Q} \quad (\text{A.11})$$

For completeness, we also have the dispersion-free and non-causal absorption model of Futterman (1962), which corresponds to

$$A_{Futt} = 1 \quad B_{Futt} = \frac{1}{Q} \quad (\text{A.12})$$

Ricker wavelet in the synthetics

In order to get the synthetic seismogram in time domain by inverse Fourier transform of the complex reflection coefficient K , each component of K (Eq.(26) is multiplied by a sampled Ricker wavelet in frequency domain:

$$Sr_w = (2/\sqrt{\pi}) \frac{f^2}{f_c^3} \exp\left(-\frac{f}{f_c}\right)^2 \quad (\text{A.13})$$

This Ricker wavelet is a zero-phase wavelet and is non-causal. The frequency f_c is called the center frequency and will vary.

Appendix 2

To apply least-square inversion, Eq. (29) can be written in vector and matrix notation in short as

$$\vec{K} = M \vec{r} \quad (\text{A14})$$

where

$$\vec{K} = \begin{bmatrix} K_{n+1}(\omega_0, 0) \\ K_{n+1}(\omega_1, 0) \\ \vdots \\ K_{n+1}(\omega_{NT-1}, 0) \end{bmatrix} \quad \vec{r} = \begin{bmatrix} r_{n,0} \\ r_{n,1} \\ \vdots \\ r_{n,NT-1} \end{bmatrix}$$

$$M = \Delta\tau \begin{pmatrix} \exp(-\varphi(\omega_0, 0)(1 - K_{0,n}^2)) & \exp(-\varphi(\omega_0, \Delta\tau)(1 - K_{1,n}^2)) & \dots & \exp(-\varphi(\omega_0, (NT-1)\Delta\tau)(1 - K_{n,n}^2)) \\ \exp(-\varphi(\omega_1, 0)(1 - K_{0,n}^2)) & \exp(-\varphi(\omega_1, \Delta\tau)(1 - K_{1,n}^2)) & \dots & \exp(-\varphi(\omega_1, (NT-1)\Delta\tau)(1 - K_{n,n}^2)) \\ \vdots & \vdots & \dots & \vdots \\ \vdots & \vdots & \dots & \vdots \\ \exp(-\varphi(\omega_{NT-1}, 0)(1 - K_{0,n}^2)) & \exp(-\varphi(\omega_{NT-1}, \Delta\tau)(1 - K_{1,n}^2)) & \dots & \exp(-\varphi(\omega_{NT-1}, (NT-1)\Delta\tau)(1 - K_{n,n}^2)) \end{pmatrix} \quad (\text{A15})$$

\vec{K} is a (N \times 1) vector, M is a (N \times N) matrix and \vec{r} is a (N \times 1) vector. Let \vec{K} be the desired seismic output data while the actual output from Eq. (A14) is $\vec{S} = M \vec{r}$. We want to compute a reflectivity per depth unit series \vec{r} such that the difference $\vec{\Sigma}$ between the actual output \vec{S} and the predicted seismic output data \vec{K} is minimum in the least square sense. Therefore, the error $\vec{\Sigma}$ with respect to parameter vector \vec{r} is $\vec{\Sigma} = \vec{K} - \vec{S} = \vec{K} - M\vec{r}$. And the cumulative squared error:

$$\begin{aligned} \vec{\Sigma}^T \vec{\Sigma} &= (\vec{K} - M\vec{r})^T * (\vec{K} - M\vec{r}) = \\ &(\vec{K}^T * \vec{K} - \vec{K}^T M\vec{r}) - r^T M^T K^T + (\vec{r}^T M^T * M\vec{r}) \end{aligned} \quad (\text{A16})$$

Where T denotes matrix transpose and * denotes complex conjugate.

We want to estimate a reflectivity per depth unit series \vec{r} such that the quantity $\vec{\Sigma}^T \vec{\Sigma}$ is minimum. This condition leads to setting the derivative of $\vec{\Sigma}^T \vec{\Sigma}$ with respect to \vec{r} to zero. Differentiate both sides of eq. (A16) with respect to \vec{r} and observe the requirement for least square procedure minimization that

$$\frac{\delta \vec{\Sigma}^T \vec{\Sigma}}{\partial \vec{r}} = -\vec{K}^T * M + r^T * M^T * M = 0 \quad (\text{A17})$$

Because \vec{r}^{T*} is complex valued, $\frac{\delta \vec{r}^{T*}}{\delta \vec{r}} = 0$. Thus applying matrix transpose and rearranging the terms of eq. (A17)

$$\begin{aligned} (M^T * M)^T * \vec{r} &= M^T \vec{K} \Rightarrow (M^T M) \vec{r} = M^T * \vec{K} \\ \Rightarrow \vec{r} &= (M^T * M)^{-1} M^T \vec{K} \end{aligned} \tag{A18}$$

Eq (A18) will give us the reflectivity per depth unit and from this we can calculate the impedance.

Damping constant when calculating reflectivity

To further understand the inversion we need to discuss how reflectivity per depth unit is computed and the introduction of the matrix M defined in Eq.(A14). However an important aspect must be discussed first. The singularity of the matrix $M^T * M$ makes it necessary to introduce a damping constant λ when calculating r. This λ is chosen out from the ‘singular value decomposition’ (svd) of the matrix $M^T * M$. Now we get an invertible new matrix:

$$L = \text{svd}(M^T * M) \text{ giving } M^T * M + \lambda I$$

I is a unitary matrix of the same order as the matrix $M^T * M$

$$\begin{aligned} (M^T * M)^T * \vec{r} &= M^T \vec{K} \Rightarrow (M^T M) \vec{r} = M^T * \vec{K} \\ \Rightarrow \vec{r} &= (M^T * M)^{-1} M^T \vec{K} \end{aligned} \tag{A.19}$$

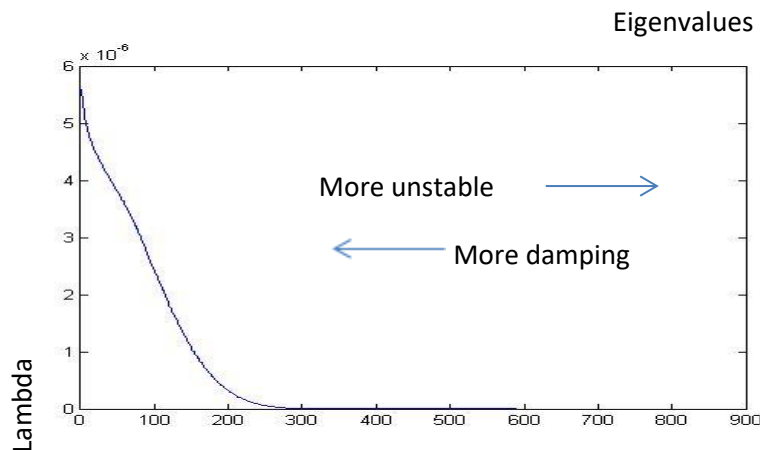


Fig.A.1 .Damping constant lambda as a function of the eigenvalues of $M^T * M$

We will choose lambda around (NT/2) eigenvalue of the matrix $M^T * M$ to be able to use it in the inversion. The output reflectivity (r) will then depend on the value of lambda and introduce damping.

Fig.A.1 shows that when we choose smaller eigenvalues lambda will increase and r is more damped. When lambda increase we found that the effect of the inversion was less and over a threshold value no effect at all. When we increase eigenvalues, lambda decrease. Then we get less damping but r is also more unstable, and can introduce noise. For all calculations in our article we choose lambda=4.8.

It should be taken care to choose the right damping constant (λ) in order to perform the inversion. The choice must be related to noise level, choice of Butterworth filtering and scaling until one gets a satisfying result. We have not discussed this here, but plan to do it in future research.